Contribution of Solar Mass Loss to the Solution the Faint Young Sun Paradox for Physically Motivated Mass Loss Prescriptions

Research Thesis

Presented in Partial Fulfillment of the Requirements for graduation "with Research Distinction in Astronomy" in the undergraduate colleges of The Ohio State University

by

Lawrence Capuder

The Ohio State University

June 2012

Project Advisors: Marc Pinsonneault, B. Scott Gaudi

ABSTRACT

I consider the maximum contribution of mass loss and uncertainties in the standard (no mass loss) solar model to the resolution to the faint young sun paradox. I first consider the degree to which the past luminosity evolution of the sun could have differed from the prediction of the standard solar model by generating solar luminosity histories using alternate input physics and variations in the solar parameters. I find negligible variations (maximum of $\sim 0.602\%$) in the solar luminosity history for reasonable variations in the input physics and solar parameters, consistent with prior work. I also consider various physically motivated and ad hoc models for the mass loss history of the sun, which can in principle resolve the paradox by making the early sun more massive, and thus more luminous. I show that for reasonable physically motivated mass loss prescriptions, the luminosity evolution for most of the sun's lifetime is unaffected. This upper limit on potential mass loss of the sun can be used to calibrate the extent to which the atmosphere and surface of the early Earth must differ from the present day in order to resolve the paradox.

1. Introduction

Using the standard theories of stellar structure and evolution one can infer the past evolution of the physical properties of the sun, given the empirical constraints on its current properties (radius, age, luminosity, etc.) Assuming it stays at a constant mass, the sun would have been about 70% its current luminosity for the early Earth (Gough 1981). Thus, assuming the conditions on the early Earth were the same as today (i.e. albedo and infrared emissivity of the atmosphere were the same), the temperature on the surface of the Earth

would have been 261 K, too cold to allow liquid water. However, there is strong evidence that suggests that the early Earth possessed abundant liquid water in its early history, including the presence of lava pillows, mud cracks, and ripple marks in rocks from the Swaziland subgroup (Ramsay 1963), the abundance and composition of sediments (Donn, Donn, & Valentine 1965), and the emergence of life, which is strongly agreed upon in the scientific community to have required liquid water. This apparent contradiction is commonly referred to as the faint young sun paradox (Sagan & Mullen 1972).

Although many different solutions have been proposed, under close scrutiny, none appears capable of fully resolving the paradox on their own. Sagan and Mullen(1992) themselves proposed that increased concentrations of NH_3, a greenhouse gas, in the Earth's atmosphere could have caused the needed temperature increase. However it was later shown that ammonia is photochemically unstable without the presence of O_3, which was not present in the early atmosphere (Kuhn & Atreya 1979). CO_2, another strong greenhouse gas, would seem to be a likely candidate (Walker, Hays, & Kasting 1981). However, Rosing *et. al.*(2010) put an upper limit on the concentration of CO_2 in the early atmosphere using banded iron formations, and argued that this upper limit is too low to account for the temperature increase necessary to resolve the paradox. CH_4 is another greenhouse gas that could plausibly resolve the paradox, however it is believed that an organic haze forms at atmospheric CH_4/CO_2 ratios of higher than ~ 0.1, thus increasing the albedo of the Earth, resulting in a net decrease in the overall surface temperature (Haqq-Misra et. al. 2008).

Smaller past planetary albedos have also been suggested as a mechanism to increase the temperature of the Earth. Factors that could contribute to a smaller albedo are a lack of vegetation, a smaller surface area of land relative to ocean, and the presence of different cloud condensation nuclei (Rosing et. al. 2010). However, Kasting (2010) has argued that these effect are insufficient to raise the surface temperature of the Earth above the freezing

point of water when one considers the positive ice-albedo feedback.

The proposed solution we consider here is mass loss from the sun. Mass loss affects solar luminosity because luminosity is strongly proportional to mass. Furthermore, as the sun loses mass, the planetary orbits move out, and thus the Earth would have been orbiting closer to a sun that was more massive in the past. However, if the current mass loss rate of $2-3\times10^{-14}\mathrm{M}_{\odot}$/year (Feldman et al. 1977) remained constant over time, the total amount of mass lost by the sun during its 4.57 Gyr history would have only been 0.05% of the current solar mass, which would negligibly affect the solar flux at the Earth. A study done by Wood et. al.(2002) attempted to estimate the mass loss history of the sun by comparing it to that of similar main sequence stars inferred from the Lyα emission arising from the shock created when stellar wind collides with the ambient interstellar medium. This study concluded that if the mass loss history of the sun were similar to the solar analogues, it would have been many orders of magnitude too small to resolve the faint young sun paradox.

It is possible that the mass loss history of the sun is atypical (Wood et. al. 2002). Past papers, such as Minton & Malhotra(2007), have explored a variety of ad hoc past solar mass loss histories and assessed how they would affect the temperature of the Earth. They determined that mass loss has the possibility of resolving the faint young sun paradox. Here I perform a similar type of analysis, however I will primarily consider physically motivated mass loss models and assess the degree to which those can solve the Faint Young Sun Paradox. Furthermore, I will attempt to put constraints on the possible mass loss history of the sun using a variety of empirical constraints.

In Section 2, this paper discusses the input physics and parameters that go into a standard solar model, as described in Pinsonneault et. al. (2010). We will then discuss the uncertainties in the standard solar luminosity histories by considering deviant models. In Section 3, I will discuss limits on mass loss, the accuracy of the equations used to model the

solar luminosity and mass loss effects in Minton & Malhotra 2007, and the effects of constant and physically motivated mass loss models on the faint young sun paradox.

2. Solar Luminosity History

In Section 2.1, I will define a "standard solar model," the solar model constructed using the best available physics and input data. I will then discuss deviant models, the past evolution of the sun due to uncertainties in the input physics and empirical constraints, in Section 2.2, for the purpose of determining the uncertainty in the overall luminosity history of the sun. This process shows that the uncertainty in the standard solar luminosity history is very small and thus contributes negligibly to the resolution of the faint young sun paradox. All of the models are calibrated to have the current luminosity, radius, and surface Z/X at the current age of the sun, except for the deviant models in which these parameters are varied explicitly.

2.1. Standard Model

The input physics of my standard solar model use OPAL 2006 equations of state (Rogers & Nayfonov 2002 with alterations on their web site) and OP opacity tables (Badnell et al. 2005), which were supplemented by Ferguson *et. al.* (2005) molecular opacities for temperatures below 10^4 K. The model was calculated using the usual mixing length formalism to determine convective flux. I used a diffusion scale factor of 0.8 (Thoul et al. 1994) to account for mixing (Bahcall 2001), Allard boundary conditions (Hauschildt et al. 1999), and Adelberger et al. (2010) nuclear cross sections. No mass loss was considered in the standard model. The current value of the solar luminosity to which the models were calibrated to was 3.8418×10^{33} erg/sec (Fröhlich & Lean 1998). The current radius used was 6.9598×10^{10} cm.

The current age of the sun used was 4.57 Gyr (Bahcall & Pinsonneault 1995). The models were also calibrated to a surface Z/X (metal abundance to hydrogen abundance ratio) of 0.0229 (Greveese & Sauval 1998) respectively. The solar luminosity history based on the standard solar model is shown in Figure 1.

2.2. Uncertainties in Solar Luminosity History

Uncertainties in the solar luminosity history were calculated by simulating deviant solar models, in which one aspect of the standard solar model was changed, and then combining each of these models' time-dependent deviations from the standard solar model. The following is a list of the deviant models considered:

Equations of state provide a mathematical relationship between temperature, pressure, and density. These are applied to the code through a set of tables defined by various sources. The OPAL96 case was generated by replacing the OPAL 2006 equations of state tables with OPAL 1996 tables (Rogers, Swenson, & Igesias 1996) equations of state. The OPAL01 case was generated by replacing the OPAL 2006 equations of state tables with OPAL 2001 (Rogers & Nayfonov 2002) equations of state tables.

Opacity describes the interaction of light and matter, which depends on chemical composition. These interactions are determined by theoretical quantum mechanics calculations. The OPAL Opacities case was generated by replacing the OP opacities with OPAL opacitices, which is a different set of theoretical calculations (Iglesias & Rogers 1996).

Heavy elements sink relative to lighter elements in a gravitational potential. This effect causes a reduction of helium and heavy metal abundances on the surface of the sun on the order of magnitude of 10%, thus slightly raising the core metallicty. The Diffusion Factor Plus case was generated by altering the diffusion scale factor by adding one standard deviation of

0.3, giving a diffusion scale factor of 1.1(Thoul et al. 1994). The Diffusion Factor Minus case was generated by altering the diffusion scale factor by subtracting one standard deviation of 0.3, giving a diffusion scale factor 0.5 (Thoul et al. 1994).

Different atmospheric properties create different boundary conditions for the simulations. The Gray BC case was generated by replacing Allard boundary conditions with Gray boundary conditions. The Kurucz BC case was generated by replacing Allard boundary conditions Kurucz boundary conditions.

A nuclear reaction cross section is the effective area which governs the likelihood of interaction between particles. These cross sections have a strong impact on how much fusion occurs in the core of the sun and therefore how much energy is generated in the core. This energy generation has a strong impact on the equations of state and on the sun's overall luminosity. The $S_{1,1}(0)$ Plus case was generated by altering the $S_{1,1}(0)$ nuclear cross section by adding one standard deviation as cited in Adelberger et. al (2010). The $S_{1,1}(0)$ Minus case was generated by altering the $S_{1,1}(0)$ nuclear cross section by minus σ as cited in Adelberger et. al (2010). The $S_{3,3}(0)$ Plus case was generated by altering the $S_{3,3}(0)$ nuclear cross section by adding one standard deviation as cited in Adelberger et. al (2010). The $S_{3,3}(0)$ Minus case was generated by altering the $S_{3,3}(0)$ nuclear cross section by minus σ as cited in Adelberger et. al (2010). The $S_{3,4}(0)$ Plus case was generated by altering the $S_{3,4}(0)$ nuclear cross section by adding one standard deviation as cited in Adelberger et. al (2010). The $S_{3,4}(0)$ Minus case was generated by altering the $S_{3,4}(0)$ nuclear cross section by minus σ as cited in Adelberger et. al (2010). The $S_{1,14}(0)$ Plus case was generated by altering the $S_{1,14}(0)$ nuclear cross section by adding one standard deviation as cited in Adelberger et. al (2010). The $S_{1,14}(0)$ Minus case was generated by altering the $S_{1,14}(0)$ nuclear cross section by minus σ as cited in Adelberger et. al (2010).

The current properties of the sun are measured with an amount of uncertainty based on

whatever method was used to measure it. The $L_\odot$ Plus case was calibrated to one standard deviation above the accepted value of the current solar luminosity. $\sigma = 0.8$ percent, giving a current solar luminosity of 3.87253×10^{33} erg/sec. The $L_\odot$ Minus case was calibrated to one deviation below the accepted value of the current solar luminosity. $\sigma = 0.8$ percent, giving a current solar luminosity of 3.81107×10^{33} erg/sec. The $R_\odot$ Alt case was calibrated to an alternative solar radius of 6.95508×10^{10} cm (Brown & Christensen-Dalsgaard 1998). The $Age_\odot$ Plus case was calibrated to one standard deviation above the accepted value of the current solar age. $\sigma = 0.02$ Gyr, giving a current solar age of 4.59 Gyr(Bahcall & Pinsonneault 1995). The $Age_\odot$ Minus case was calibrated to one deviation below the accepted value of the current solar age. $\sigma = 0.02$ Gyr, giving a current solar age of 4.55 Gyr(Bahcall & Pinsonneault 1995).

The initial conditions necessary for the models to converge to the current luminosity, radius, and surface Z/X are shown in Table 1.

Figures 2-3 show the deviation of the solar luminosity from the standard model as a function of time for the various alternative models listed above the sum of all the uncertainty sources added in quadrature not including the uncertainty in the current luminosity of the sun. The deviations in the luminosity from the standard solar model generally get smaller as the age of the sun approaches the current age, 4.57 Gyr (Bahcall & Pinsonneault 1995), except for the $Age_\odot$ plus and $Age_\odot$ minus models, as can be seen on Figures 2-3. These models do not approach zero uncertainty at 4.57 Gyr because they were calibrated to a different current age of the sun. For two of the individual models, the Kurucz BC model and the $R_\odot$ Alt model, the deviations from the standard model increase with time. However, the uncertainty is small enough in both of these models that this is most likely due to numerical errors.

Figure 4 shows the uncertainty due to the uncertainty in the current luminosity of the sun and the total sum of all the uncertainty sources added in quadrature. The uncertainty

in the current luminosity of the sun also does not converge to zero at 4.57 Gyr because it was calibrated to a different value for the current luminosity of the sun than the standard model. The uncertainty in the current luminosity of the sun dominates over the effects of the other sources of uncertainty on the luminosity history of the sun.

I conclude that the uncertainties in input physics and current solar parameters affect the solar luminosity history by amounts that are clearly much too small to resolve the faint young sun paradox on their own. Indeed, these uncertainties negligibly affect the past solar luminosity evolution.

3. Mass Loss

3.1. Luminosity Approximation

I compared detailed numerical models with an analytical fit. I found that the analytical fit approximates luminosity very well. This fit was not used in our calculations, but might be a faster way to determine luminosity in the future in some situations. Minton & Malhotra (2007) adopt a mass-luminosity relation of the form $L \alpha M^{\beta}$,with a power law index of $\beta = 4.75$. I find that $\beta = 4.25$ provides a better fit to my results and so adopt this value. Combining this relation with an inverse linear dependance of the luminosity with time found by Gough 1981, results in the following expression,

$$\frac{L(t)}{L_{\odot}} = \left[1 + \frac{9}{25}\left(1 - \frac{t}{t_{\odot}}\right)\right]^{-1} \left[\frac{M(t)}{M_{\odot}}\right]^{4.25} \quad (1)$$

where $M(t)$ is the mass of the sun at time t and $t_{\odot}$ is the current age of the sun (Minton & Malhotra 2007). Note also that I adopt a factor of 9/25, which I find provides a better approximation than the value of 2/5 reported by Gough 1981. Figure 5 shows the deviation between Equation 1 from the exact luminosity evolution assuming simulated mass loss cases. Figure 5 shows that the relation from Equation 1 is a sufficient approximation for my considerations.

Table 1: The initial surface metal to hydrogen abundance ratio, initial hydrogen content, and mixing length are given for the standard and deviant models considered in this paper that produce the current luminosity, radius, and surface metal to hydrogen abundance ratio at the current age of the sun.

Model	$(Z/X)_o$	X_o	α
Standard	0.018336	0.71033	1.912
$S_{3,4}(0)$ Plus	0.018315	0.70100	1.917
$S_{3,4}(0)$ Minus	0.018349	0.71077	1.907
$S_{3,3}(0)$ Plus	0.01833	0.71047	1.911
$S_{3,3}(0)$ Minus	0.018327	0.71026	1.914
$S_{1,1}(0)$ Plus	0.01830	0.71009	1.920
$S_{1,1}(0)$ Minus	0.01837	0.71066	1.904
$S_{1,14}(0)$ Plus	0.01834	0.71030	1.912
$S_{1,14}(0)$ Minus	0.01834	0.71037	1.912
$R_\odot$ Alt	0.01833	0.71038	1.918
OPAL96	0.01834	0.71072	1.890
OPAL01	0.01834	0.71020	1.834
$L_\odot$ Plus	0.01831	0.70962	1.831
$L_\odot$ Minus	0.01835	0.71112	1.897
OPAL opacities	0.01834	0.70968	1.902
Diffusion Factor Plus	0.01900	0.70728	1.948
Diffusion Factor Minus	0.01765	0.71365	1.872
Kurucz BC	0.01833	0.71038	1.920
Gray BC	0.018344	0.710270	1.825
$Age_\odot$ Plus	0.01833	0.71058	1.914
$Age_\odot$ Minus	0.01833	0.71021	1.910
Z/X Plus	0.01992	0.70153	1.915
Z/X Minus	0.01672	0.72006	1.907

3.2. Rough Constraints on Mass Loss

We can set maximum and minimum bounds on the mass loss from the sun independent of solar models. If the solar flux at Earth had been $\gtrsim$ 10 % higher, corresponding to an upper limit on the early mass of $1.07M_\odot$, the Earth would have lost its water due to a moist greenhouse atmosphere in which water reaches the stratosphere and is lost by UV

dissociation and the subsequent escape of hydrogen to space (Kasting 1988). This process is thought to be what had occurred to Venus (Kasting & Pollack 1983).

A lower limit on mass loss can be determined by considering the sun's conversion of mass into energy and radiating it away, which can be determined by the relation $\Delta E = L\Delta t = \Delta M c^2$, where ΔE is the total energy radiated away, L is the average solar luminosity including neutrino luminosity, Δt is the time duration of nuclear burning, ΔM is the total mass converted to energy, and c is the speed of light. For the standard model, the average luminosity of the sun is about 0.85 times the current solar luminosity, giving $\Delta M \approx 3 \times 10^{-4} M_{\odot}$, which has a negligible effect on the solar luminosity history. These constraints are weak and therefore can not rule out mass loss as a possible solution to the faint young sun paradox.

More stringent constraints imposed on mass loss histories come from scalar and heliosiesmological constraints. These constraints can be calculated by comparing quantities predicted by models which vary the mass loss history of the sun against actual measured quantities and their uncertainties. I did this with the scalar quantities of surface helium (Y_{surf}), radius of the convective zone(R_{CZ}), beryllium-7 neutrino flux, and boron-8 neutrino flux at the current age of the sun. The uncertainties in the scalar quantities were derived by summing the deviations from the standard model of all of the deviant non-rotating models from Section 2.2 in quadrature. Figures 10-13 show these fraction deviations as a function of initial solar mass for the constant mass loss cases. These plots will be analyzed more in Section 3.3.3. Heliosiesmology predicts predicts a certain observed sound speed profile, which can be extracted from the models as well and would therefore also be able to test the models. The heilioseismolgy, however, is unlikely to give much different results from the scalar constraints and therefore was not analyzed in this paper.

Lithium-7 abundance also provides an upper bound on past solar mass loss. A higher

mass loss in the past means that more Lithium-7 was stripped from the sun in the solar wind. If too much Lithium-7 was stripped, the observed Lithium-7 abundance of the sun could not occur (Sackmann & Boothroyd 1993).

3.3. Solar Mass Loss History

Mass loss is likely linked to the solar wind, which occurs due to particles following the sun's magnetic field lines If the current mass loss rate of $2 - 3 \times 10^{-14} M_{\odot}$/year (Feldman et al. 1977) remained constant over time, the total amount of mass lost by the sun during its 4.57 Gyr history would be only 0.05% of the total solar mass, which would negligibly affect the solar flux at the Earth. However, evidence of higher past solar mass loss exists. This mass loss is likely linked to the solar wind, which occurs due to particles following the sun's magnetic field lines Wood et. al.(2002) studied the Lyα emission where the stars stellar wind collided with the interstellar hydrogen gas surrounding the star. From this measurement, the X-Ray luminosity of the star can be deduced, which is a measure of coronal heating. **They find a correlation between mass loss rate and X-Ray luminosity. X-Ray luminosities of up to 1000 times the sun's current luminosity have been measured for sun-like stars. However, Wood et. al. did not find enough mass loss to matter.**

Stepping away from observed and physically motivated rates, the impact of more general mass loss perscriptions can be considered. Past papers, such as Minton & Malhotra(2007), have explored various past solar mass loss histories and how they would affect the temperature of the Earth. They determined that mass loss has the possibility of resolving the faint young sun paradox. I did a similar type of analysis, however I considered physically motivated mass loss models and attempted to put upper limits on this mass loss.

3.3.1. Physically Motivated Mass Loss Models

Here I consider physically motivated mass loss models. The largest contribution to the current solar mass loss is through the solar wind, which occurs due to particles following the sun's magnetic field lines. The mass loss rate of the solar wind depends on the strength of the magnetic field lines of the sun, which depend on the sun's angular momentum. Therefore, the more angular momentum the sun has, the higher its mass loss rate. I account for these through the following expression:

$$\frac{dM}{dt}(t) = \frac{dM_{\odot}}{dt}\left(\frac{\omega(t)}{\omega_{\odot}}\right)^{P} \tag{2}$$

where ω represents the rotation rate, $\frac{dM_{\odot}}{dt}$ represents the current mass loss rate of the sun, and P represents the scaling relation between mass loss and rotation, which can be a factor between 2-3. Therefore, in order to discuss the mass loss history of the sun according to Equation 2, I must first discuss the rotation history of the sun.

The rotation history used is prescribed by Denissenkov et al.(2010). Young sun-like stars' spin increases as mass from the disk accretes onto them. Then once on the main sequence, the sun-like stars lose angular momentum due to mass loss. Denissenkov et al.(2010) gives a range of possible rotation histories for solar-type stars depending on the initial mass and rotation rate. These histories can vary significantly for a young star, but after about 1 Gyr the different rotation histories converge.

I considered three different physically motivated mass loss cases. One case was where the sun started as a fast spinner and had a mass loss prescription according to Equation 2 with $P = 3$. Another was where the sun started as a fast spinner and had a mass loss prescription according to Equation 2 with $P = 2$. The last case was where the sun started as a slow spinner and had a mass loss prescription according to Equation 2 with $P = 3$. It is unknown whether the sun started as a slow spinner or a fast spinner, however my results

Table 2: The initial surface metal to hydrogen abundance ratio, initial hydrogen content, and mixing length are given for the standard and constant mass loss models considered in this paper that produce the current luminosity, radius, and surface metal to hydrogen abundance ratio at the current age of the sun. Also shown are the surface helium ratio (Y_{surf}), convective zone depth(R_{CZ}) in solar radii, Be7 neutrino flux(F_{Be7}) in neutrinos cm^{-2} sec^{-1} $\times 10^{-10}$, and B8 neutrino flux(F_{B8}) in neutrinos cm^{-2} sec^{-1} $\times 10^{-10}$of the models at the current age of the sun.

Mass Loss Model	$(Z/X)_o$	X_o	α	Y_{surf}	R_{CZ}	F_{Be7}	F_{B8}
No Mass loss	0.018195	0.71118	1.910	0.247355	0.7153	0.4864	5.281×10^{-4}
Constant Current Mass loss	0.018343	0.71038	1.913	0.24678	0.7150	0.4895	5.358×10^{-4}
$\frac{dM}{dt}$ α ω^2, fast spinning	0.018210	0.71108	1.924	0.246363	0.7145	0.4561	4.960×10^{-4}
$\frac{dM}{dt}$ α ω^3, fast spinning	0.018210	0.71120	1.924	0.246210	0.7143	0.4516	4.882×10^{-4}
$\frac{dM}{dt}$ α ω^3, slow spinning	0.018210	0.71107	1.925	0.246176	0.7144	0.4510	4.872×10^{-4}
Constant Mass Loss Models							
Initial Mass (in solar masses)							
1.01	0.018262	0.71038	1.913	0.24682	0.7145	0.4839	5.436×10^{-4}
1.02	0.018115	0.71374	1.81	0.24680	0.7139	0.4876	5.496×10^{-4}
1.03	0.017949	0.71038	1.913	0.24666	0.7135	0.5010	5.550×10^{-4}
1.04	0.017785	0.71038	1.913	0.24654	0.7130	0.5042	5.602×10^{-4}
1.05	0.017772	0.71891	1.941	0.24624	0.7117	0.5107	5.730×10^{-4}
1.06	0.017698	0.72059	1.949	0.24599	0.7103	0.5162	5.833×10^{-4}

show that the initial rotation rate of the sun makes little difference because after about 100 Myr all initial states lead to the sun becoming a slow spinner, as demonstrated in Figures 8 and 9.

The initial conditions necessary for the models to converge to the current luminosity, radius, and surface Z/X are shown in Table 2. Also shown in Table 2 are the relevant scalar quantities.

3.3.2. Constant Mass Loss Models

The above mass loss is too small to solve the faint young sun paradox. In this section, I will evaluate the plausibility of more severe mass loss cases. As Minton & Malhotra (2007) and other previous workers have done, I considered non-physical mass loss prescriptions to resolve the Faint Young Sun Paradox. I considered simulations where the mass loss of the sun was constant until the current age was reached, where it suddenly dropped to what is observed.

Figure 6 shows the luminosity as a function of time as produced by the constant mass loss simulations. Figure 7 shows temperature as a function of time for the different constant mass loss cases considered, with a dotted line drawn at 273 K. As seen in Figure 7, a constant mass loss rate of 8.75×10^{-12} $M_\odot$/year, compared to the current mass loss rate of $2-3\times10^{-14}$ $M_\odot$/year, would be needed to resolve the faint young sun paradox.

The uncertainties in the scalar constraints discussed in Section 3.2 are graphed along with the constant model's deviations from the standard model in Figures 10-13. Figure 11 puts a loose upper limit on the constant mass loss cases. This upper limit is, however, more strict than the other upper limits discussed in Section 3.2. The constant mass loss case corresponding to an initial solar mass of $1.05M_\odot$ has a deviation of more than 2σ from the uncertainty in R_{CZ} and therefore a constant mass loss rate that high is unlikely. This puts a loose upper limit on constant mass loss cases of around 1.094×10^{-11} $M_\odot$, which is significantly higher than what is needed to resolve the Faint Young Sun Paradox. None of the other scalar constraints limit the constant mass loss models. Therefore a constant mass loss models could theoretically solve the faint young paradox and cannot be ruled out by my methods. However, such a model has no known physical motivation and is therefore extremely unlikely.

4. Conclusion

Figure 4 shows the uncertainty due to the uncertainty in the current luminosity of the sun and the total sum of all the major uncertainty sources in the solar model added in quadrature. From this, I conclude that the uncertainties in input physics and current solar parameters affect the solar luminosity history by amounts that are clearly much too small to resolve the faint young sun paradox on their own. Indeed, these uncertainties negligibly affect the past solar luminosity evolution.

Figure 9 shows temperature as a function of time for the different physically motivated mass loss cases considered with a dotted line drawn at 273 K, the freezing point of water. Figure 9 shows that the physically motivated mass loss models significantly help resolve the faint young sun paradox before 100 Myr, however are unlikely to affect the temperature of the Earth significantly after 100 Myr without using unrealistic initial rotation rates or P values from Equation 2. Figure 14 better quantifies how the physically motivated mass loss models effect the faint young sun paradox, showing the albedo needed keeping the infrared emissivity constant as a function of the age of the sun. The albedos required in the mass loss models are negligibly higher than in the standard model, thus showing that the mass loss models do little to solve the faint young sun paradox.

I conclude that there is currently no evidence of a solar solution to the faint young sun paradox. In Section 2.2, I looked at the properties of the standard solar model and determined that they were too constrained to affect the paradox. In Section 3.3.2, I determined that for currently conceivable mass loss models with physical motivation, mass loss is much too small to affect the paradox. Ad hoc mass loss models cannot be entirely ruled out based on current data, although they are extremely unlikely given that they do not have any physical motivation behind them. Future work that could potentially put a better upper limit on the ad hoc and physically motivated models include getting better measurements of

the scalar constraints discussed in Section 3.2 or by using helioseismology. Heliosiesmology predicts predicts a certain observed sound speed profile, which can be extracted from the models as well and would therefore also be able to test the models.

REFERENCES

Adelberger, E. G., et. al. 2010, Rev. Mod. Phys., 1004, 2318

Alexander, E. G., et al. 1994, Rev. Mod.Phys., 70, 1265

Badnell, N. R., Bautista, M. A., Butler, K., Delahaye, F., Mendoza, C., Palmeri, P., Zeippen, C. J., & Seaton, M. J. 2005, MINRAS, 360, 458

Bahcall, J. N., & Pinsonneault, M. H. 1995, Rev. Mod. Phys., 67, 781

Bahcall, J. N., 2001, Journal of High Energy Physics, Issue 08, pp. 014

Brown, T. M., Christensen-Dalsgaard, J. 1998, ApJ, 500, L195

Denissenkov, P. A., 2010, ApJ, 719, 28

Donn, W. L., Donn, B. D., & Valentine, W. G., Bull. Geol. Soc. Amer., 76, 287

Feldman, W. C., Asbridge, J. R., Bame, S. J., & Gosling, J. T. 1977, Colorado Assoc.Univ. Press, 351

Ferguson, J. W. 2005, ApJ, 623, 585

Fröhlich, C., & Lean, J. 1998, Geophys. Res. Lett, 25, 4377

Gough, D.O. 1981, Sol. Phys. 74, 21-34

Gough, D.O. 1981, Sol. Phys., 74, 21

Grevesse, N., & Sauval, A. J. 1998, Space Sci. Rev., 85, 161

Haqq-Misra, J. D. et. al. 2008 Astrobiology 8, 1127-1137

Hartmann, D. L. 1994, Global Phys. Climatology

Hauschildt, P.H., Allard, F., & Baron, E. 1999, ApJ, 512, 377

Iglesias, C.A., & Rogers, F.J. 1996, ApJ, 464, 943

Kasting, J. F. 1988, Icarus, 74, 472

Kasting, J. F., & Pollack, J. B. 1983, Icarus, 53, 479

Kasting, J. F., 2010 Nature, 464, 687

Kuhn, W. R., & Atreya, S. K., Icarus 37, 207-213

Minton, D.A., & Malhotra, r. 2007, ApJ, 660, 1700

Pinsonneault, M.H., & Delahaye, F., 2010, ApJ, 1005, 423

Pollack, J. B. 1979, Icarus, 37, 4794

Ramsay, J. G. 1963 Trans. Geol. Soc. S. Afr., 66, 353

Rogers, F. J., Swenson, F. J., & Iglesias, C. A. 1996, ApJ, 456, 902

Rogers, F. J., & Nayfonov, A. 2002, ApJ, 576, 1064

Rosing, M. T., Bird, D. K., Sleep, N. H. & Bjerrum, C. J. 2010, Nature 464, 744-747

Sackmann, I.J.; Boothroyd, A. I. 1993, ApJ, 418, 457

Sagan, C., & Mullen, G. 1972, Science, 177, 52

Thoul, A. A., Bahcall, J. N., & Loeb, A. 1994, ApJ, 421, 828

Walker, J. C. G., Hays, P. B. & Kasting, J. F. J. 1981, Geophys. Res. 86, 9776-9782

Wood, B. E., et. al, 2002 ApJ, 574, 412

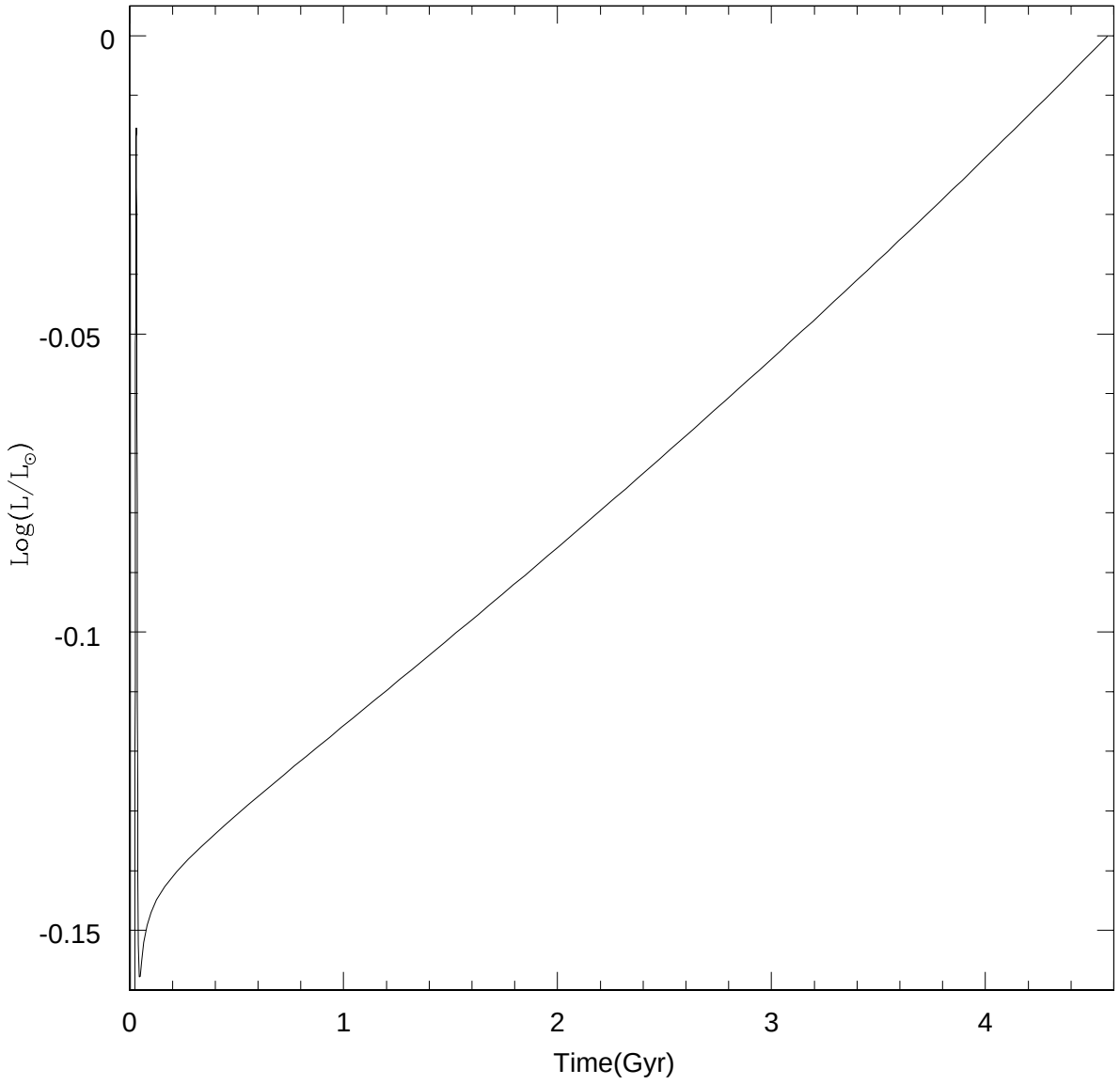

Fig. 1.— Luminosity versus time for the standard solar model

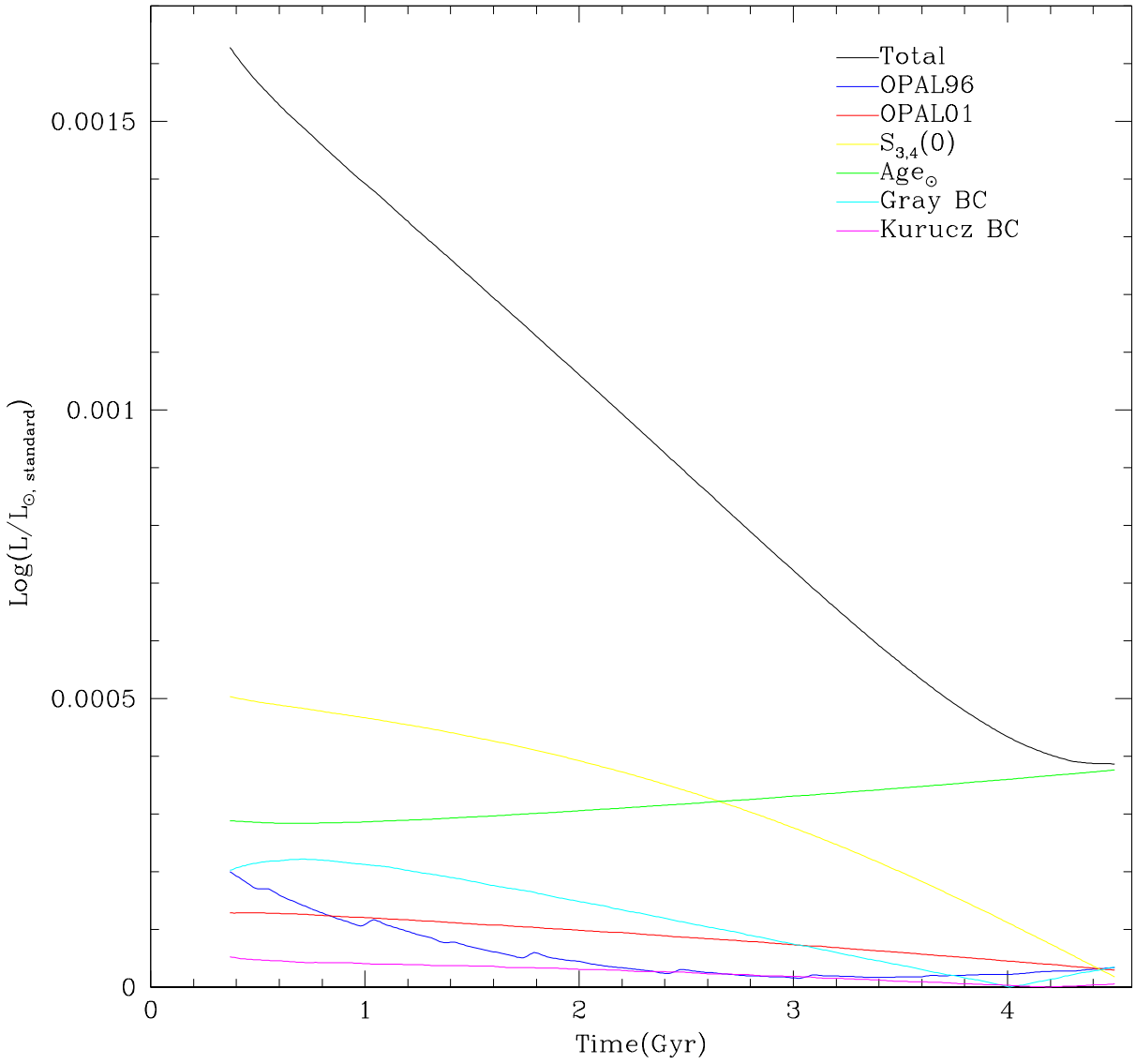

Fig. 2.— Error in standard solar model as a function of time.

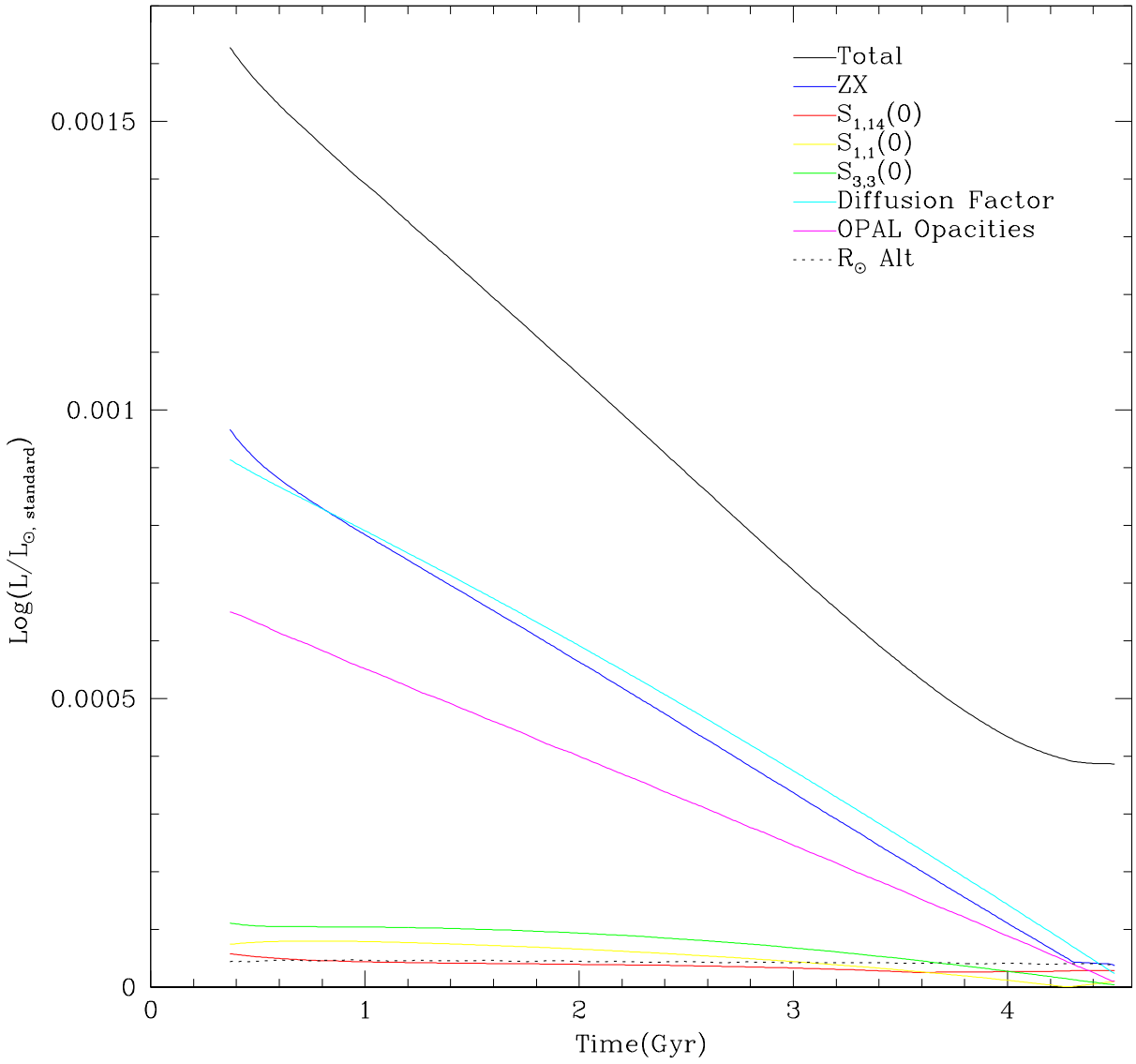

Fig. 3.— Error in standard solar model as a function of time.

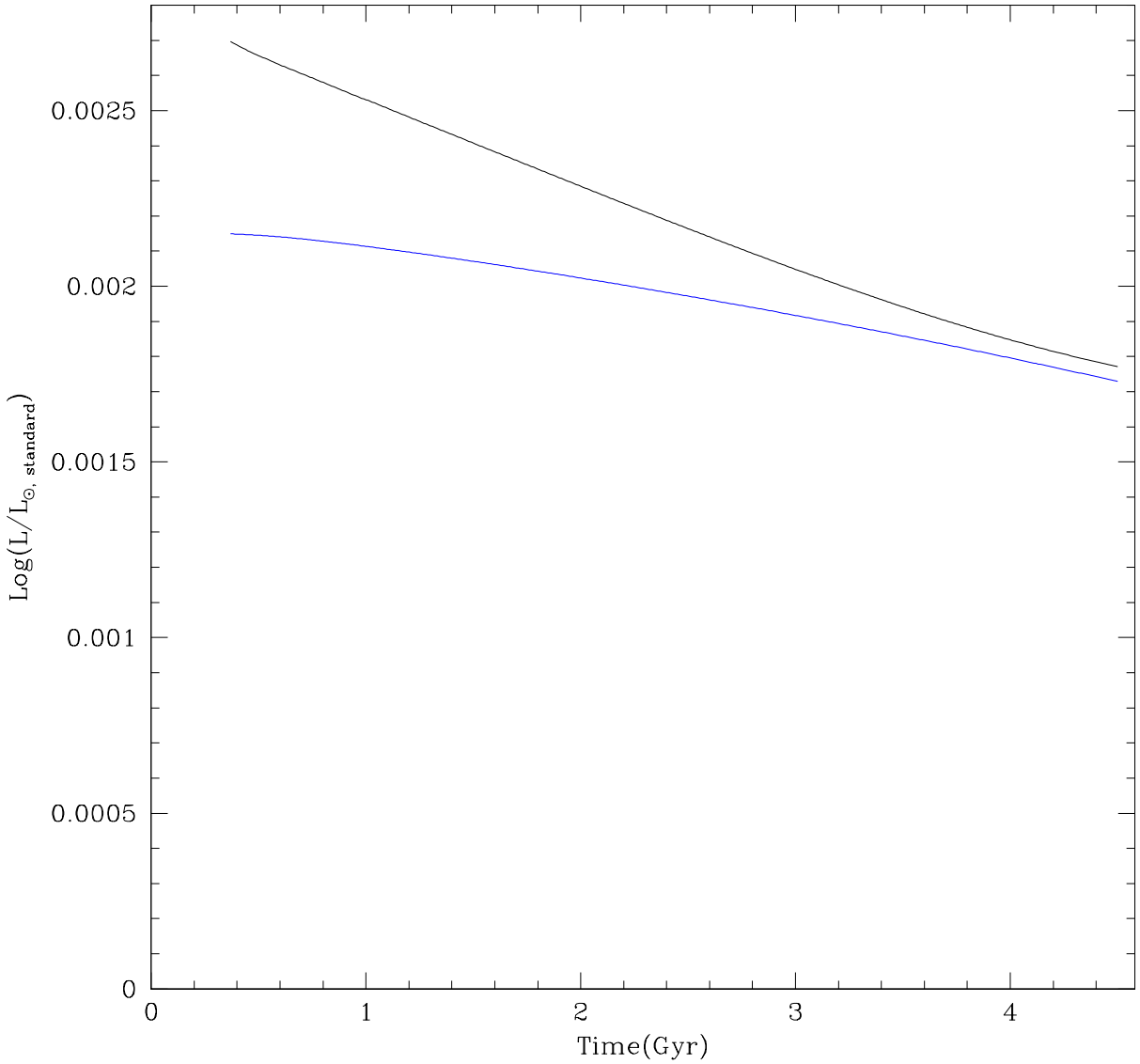

Fig. 4.— Uncertainty in standard solar model as a function of time. The total uncertainty due to the uncertainty in all of the input physics and parameters is black. The uncertainty due to the uncertainty in the current luminosity of the sun is blue.

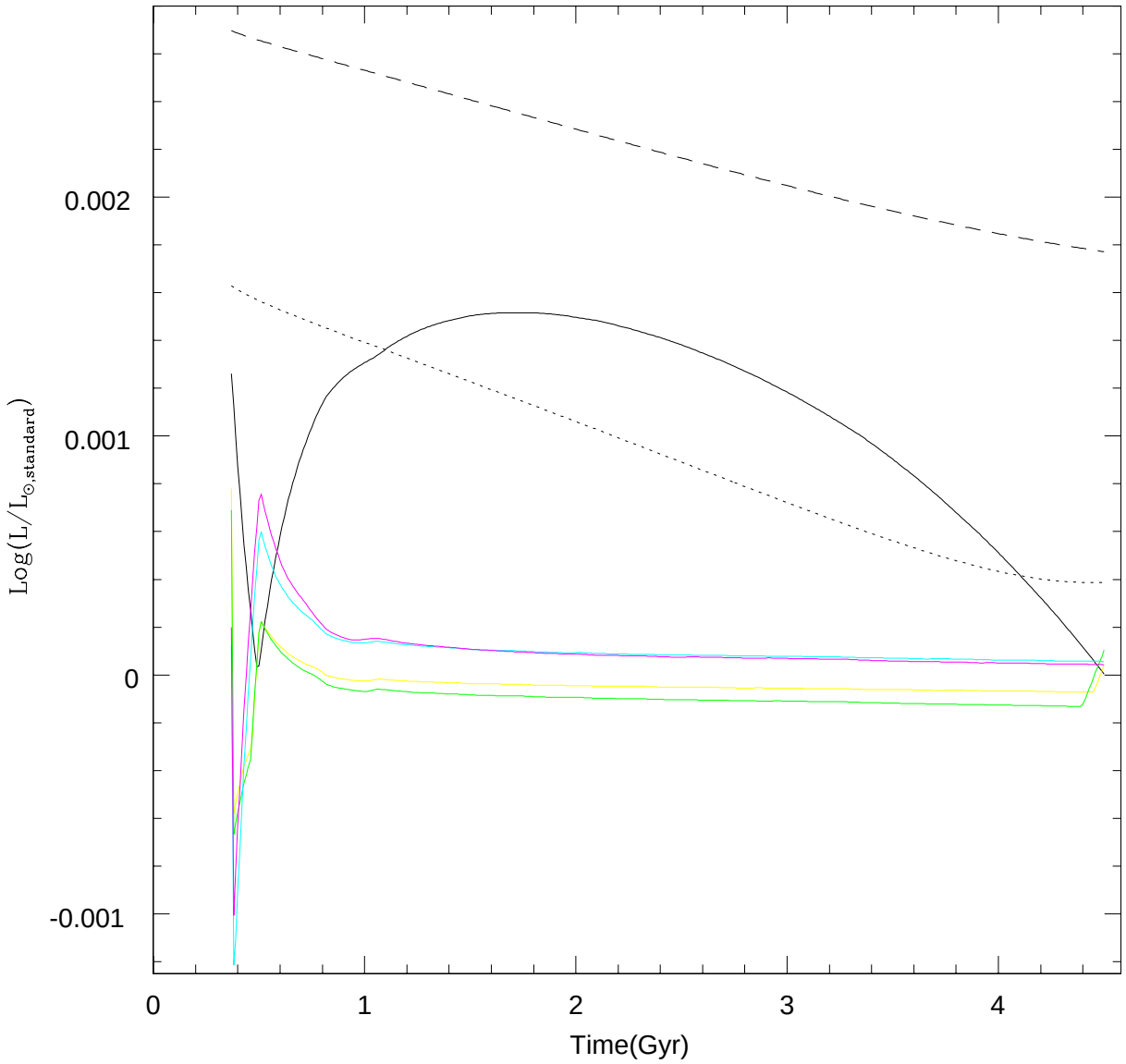

Fig. 5.— Deviation between the generated luminosity histories and the numerical result (Equation 1) for different mass loss cases. The constant mass loss cases' deviation from the numerical result is measured as a deviation from the no mass loss case. The dotted line is the one σ derived uncertainty in solar luminosity from Figures 2 and 3 that does not include the uncertainty in the current solar luminosity and the dashed line is the one σ derived uncertainty in solar luminosity from Figure 4 that includes the uncertainty in the current solar luminosity. The colored lines are as follows: Blue is initial solar mass of 1.01 times current. Red is initial solar mass of 1.02 times current. Yellow is initial solar mass of 1.03 times current. Green is initial solar mass of 1.04 times current. Cyan is initial solar mass of

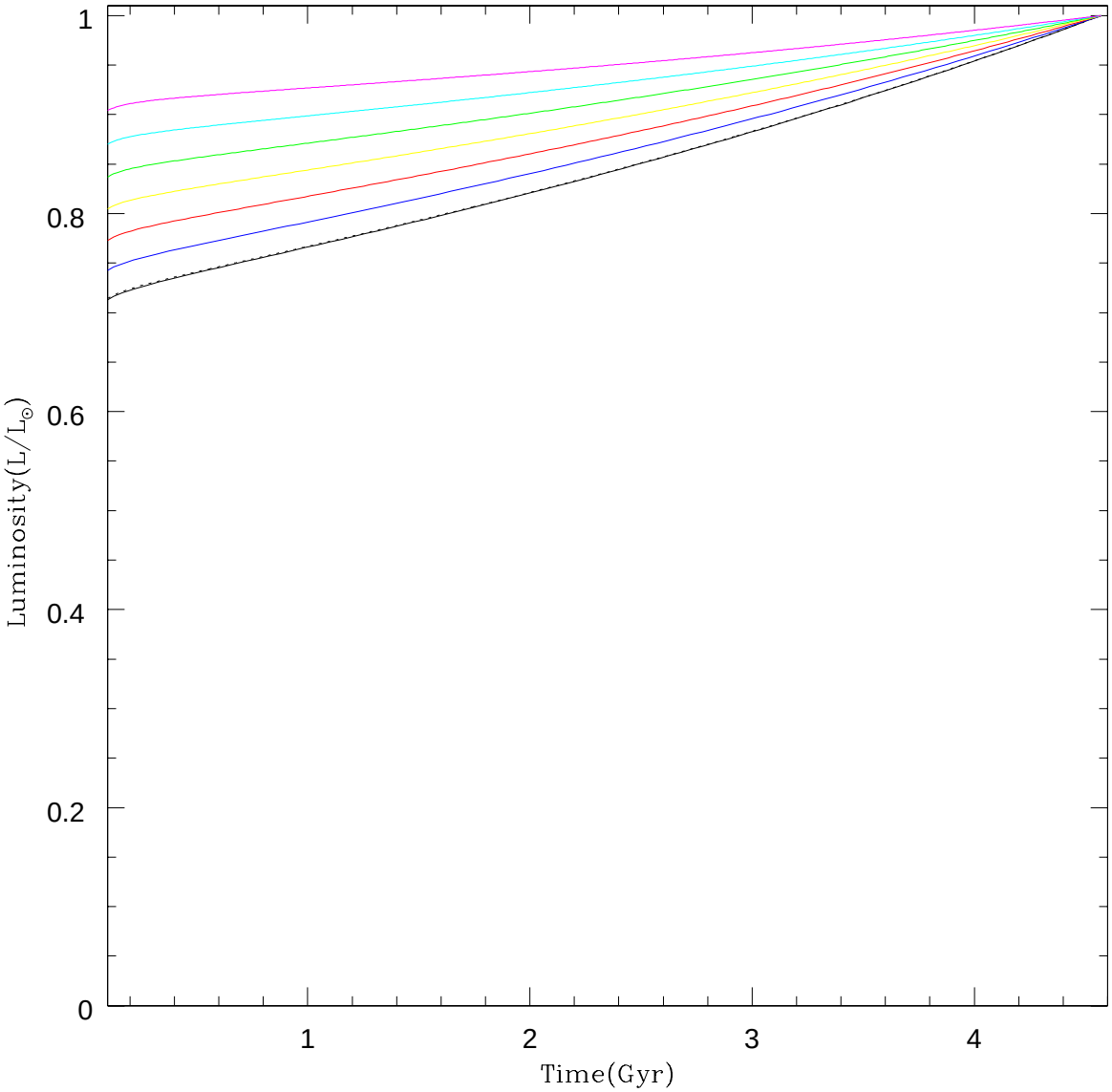

Fig. 6.— Luminosity versus time for different constant mass loss cases. The colored lines are as follows: Blue is initial solar mass of 1.01 times current. Red is initial solar mass of 1.02 times current. Yellow is initial solar mass of 1.03 times current. Green is initial solar mass of 1.04 times current. Cyan is initial solar mass of 1.05 times current. Magenta is initial solar mass of 1.06 times current.

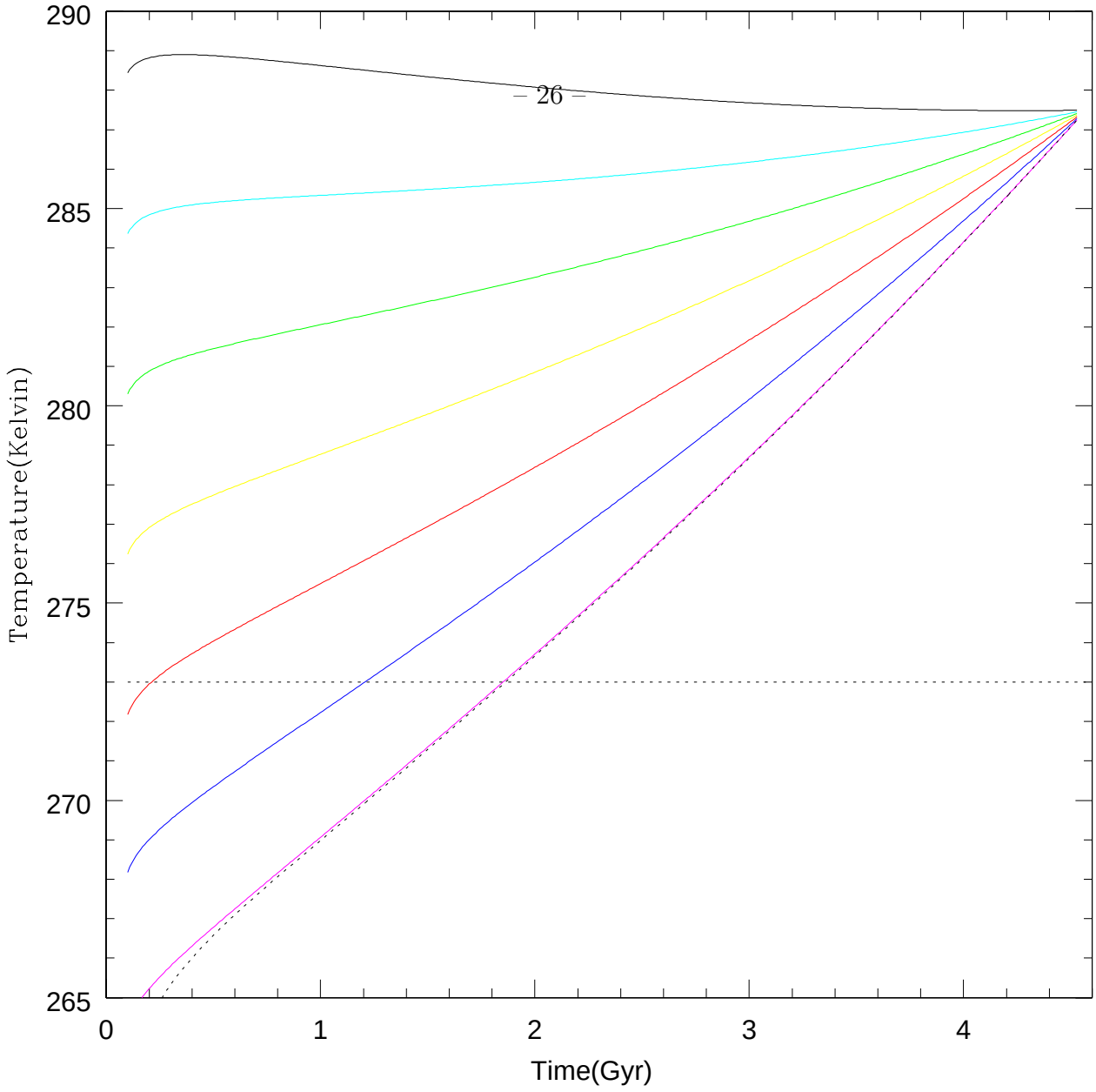

Fig. 7.— Temperature of the lower atmosphere of the Earth versus time for different mass loss cases. The dotted line is at 273 Kelvin, the freezing point of water. The lines are as follows: Dotted is standard no mass loss. Magenta assumes that the current mass loss rate was constant throughout the sun's history. Blue is initial solar mass of 1.01 times current. Red is initial solar mass of 1.02 times current. Yellow is initial solar mass of 1.03 times current. Green is initial solar mass of 1.04 times current. Cyan is initial solar mass of 1.05 times current. Black is initial solar mass of 1.06 times current.

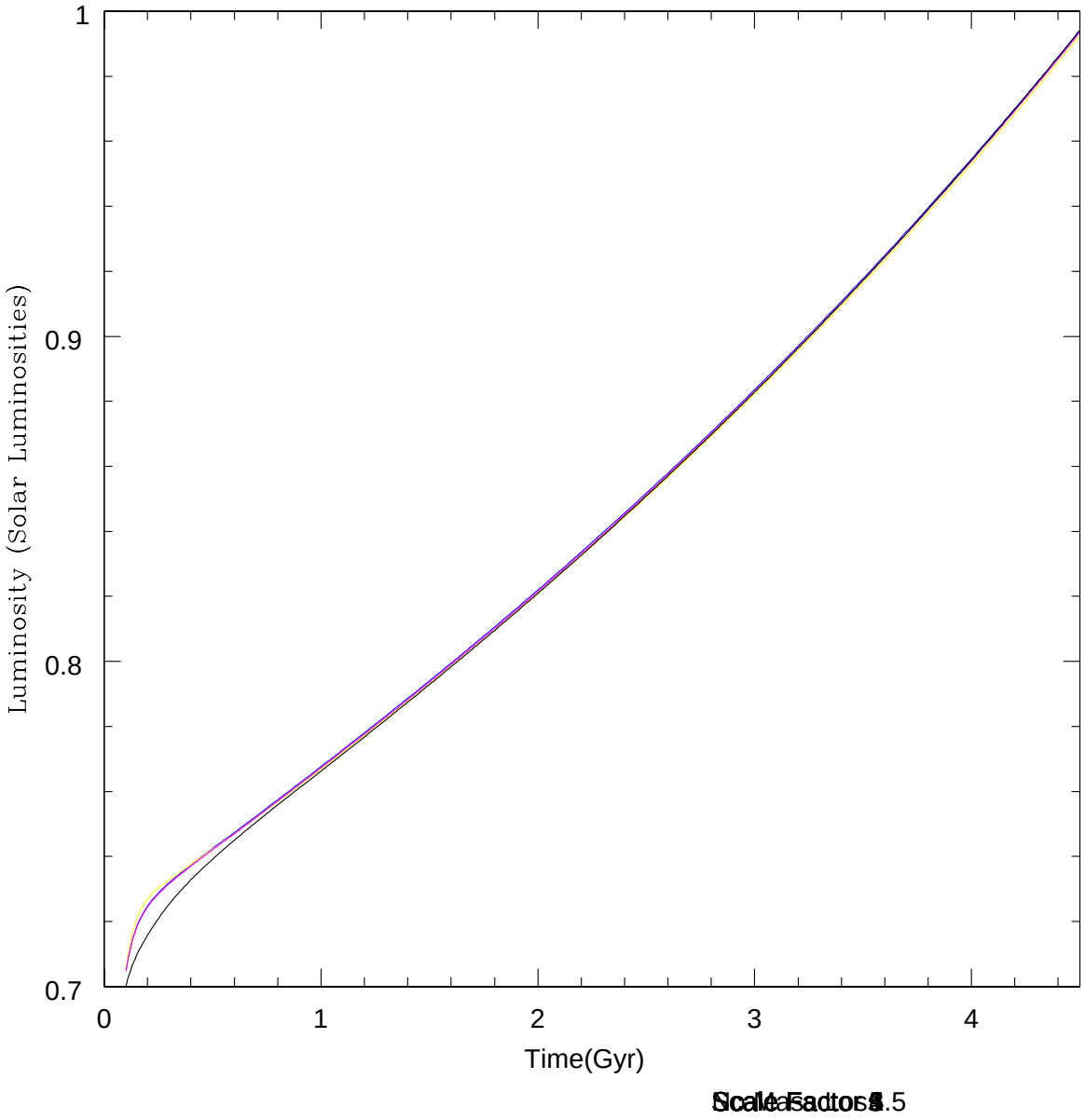

Fig. 8.— Luminosity versus time for different physically motivated mass loss models. The solid black line represents the standard no mass loss case. The lines are as follows: Black has no mass loss. Blue has $P = 2$ according to Equation 2 and starts as a fast rotator. Yellow has $P = 3$ according to Equation 2 and starts as a fast rotator. Magenta has $P = 3$ according to Equation 2 and starts as a slow rotator.

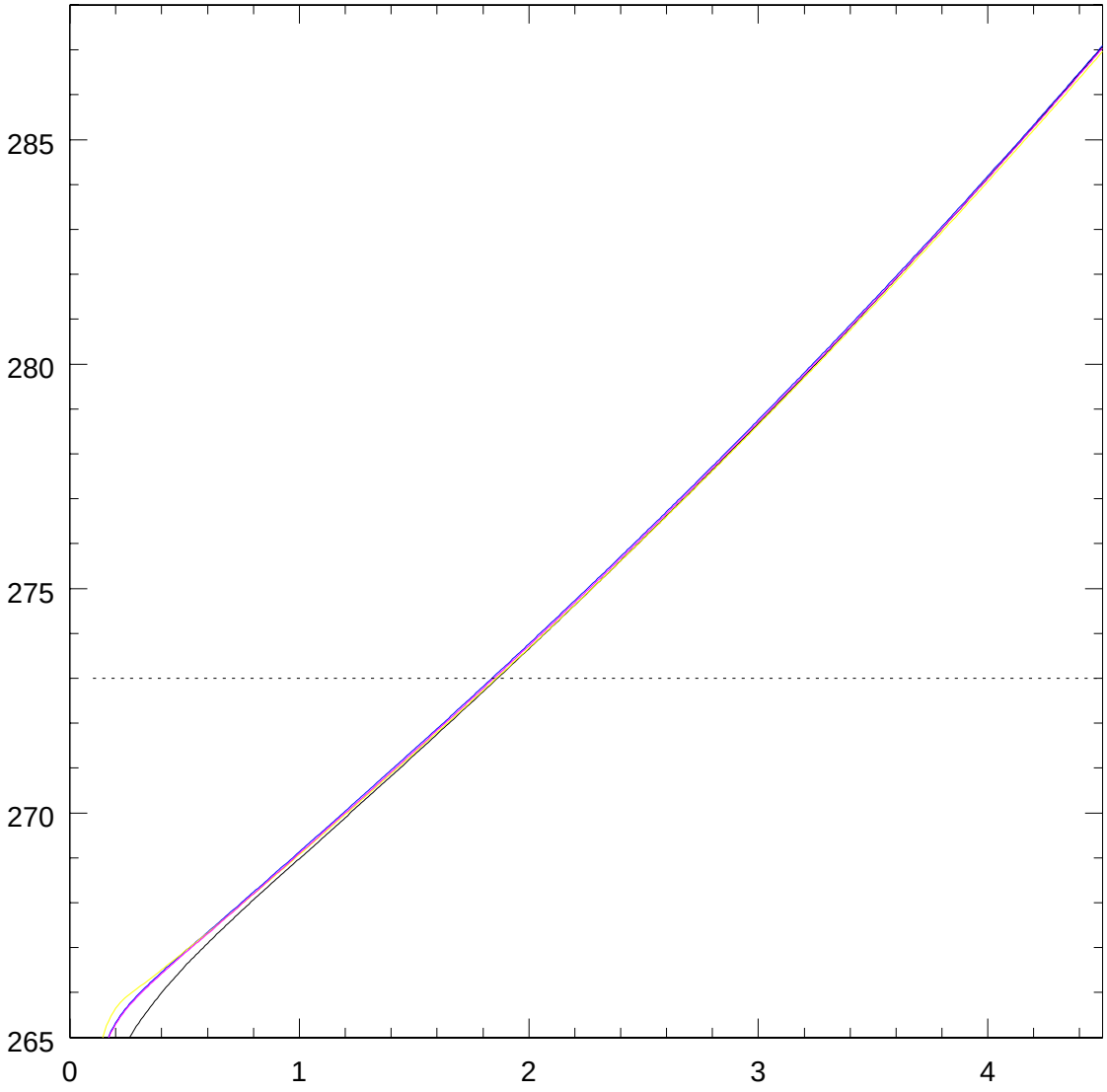

Fig. 9.— Temperature of the lower atmosphere of the Earth versus time for different physically motivated mass loss models. The dotted line is at 273 Kelvin, the freezing point of water. The lines are as follows: Black has no mass loss. Blue has $P = 2$ according to Equation 2 and starts as a fast rotator. Yellow has $P = 3$ according to Equation 2 and starts as a fast rotator. Magenta has $P = 3$ according to Equation 2 and starts as a slow rotator.

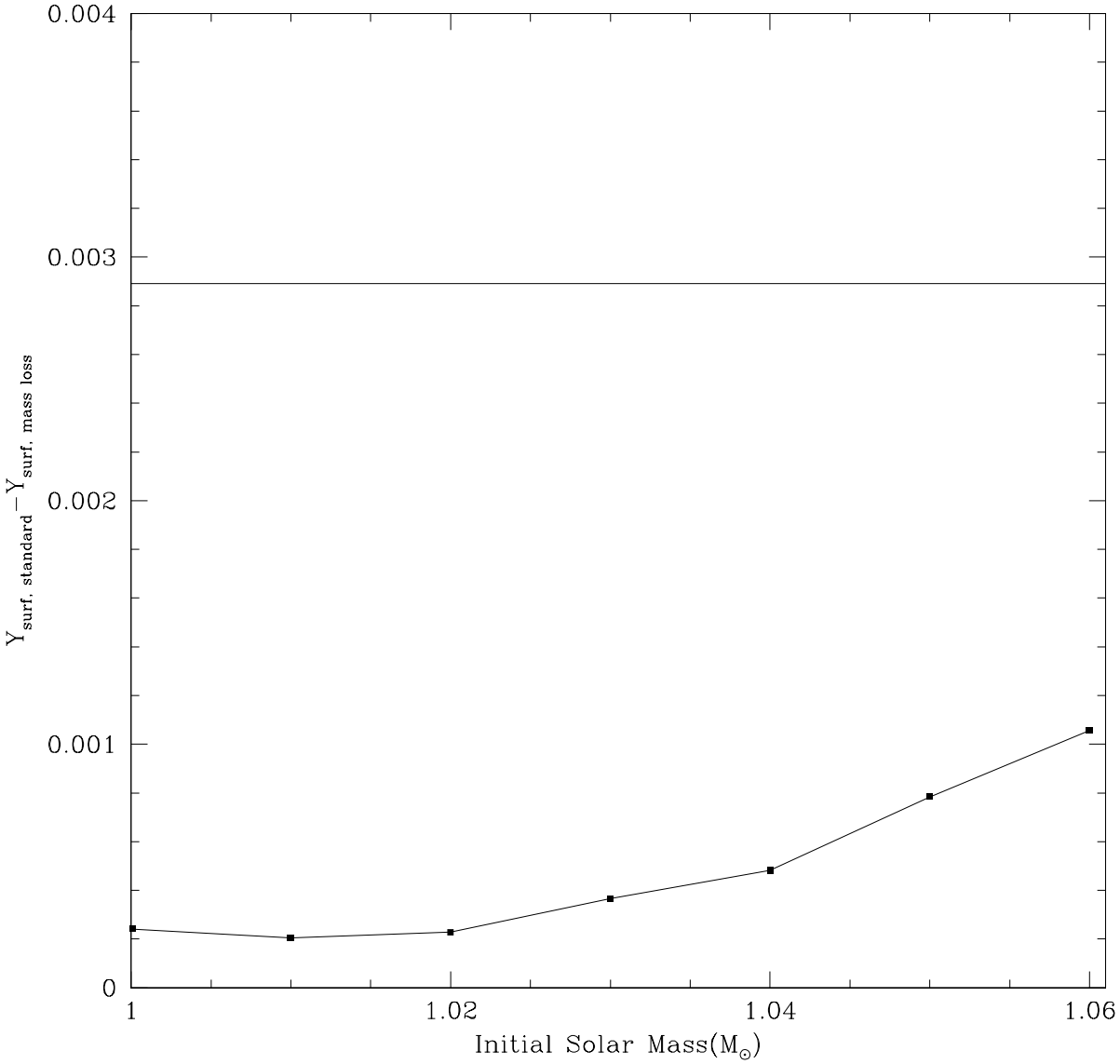

Fig. 10.— This graph shows deviation of surface helium abundance from the standard model versus initial solar mass for the constant mass loss cases. The straight line represents the derived uncertainty in the surface helium abundance.

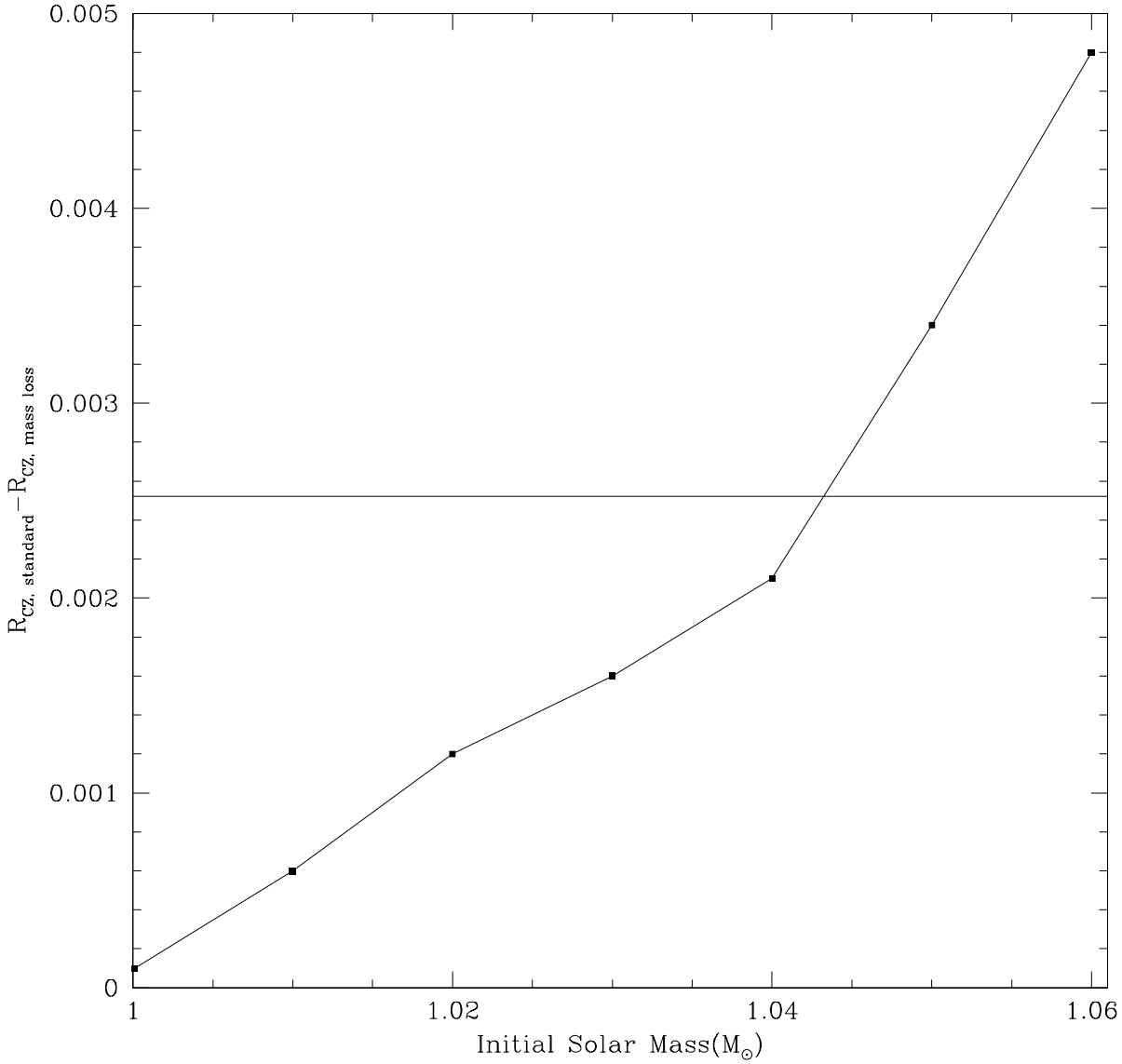

Fig. 11.— This graph shows deviation of the radius of the convective core from the standard model versus initial solar mass for the constant mass loss cases. The straight line represents the derived uncertainty in the radius of the convective core.

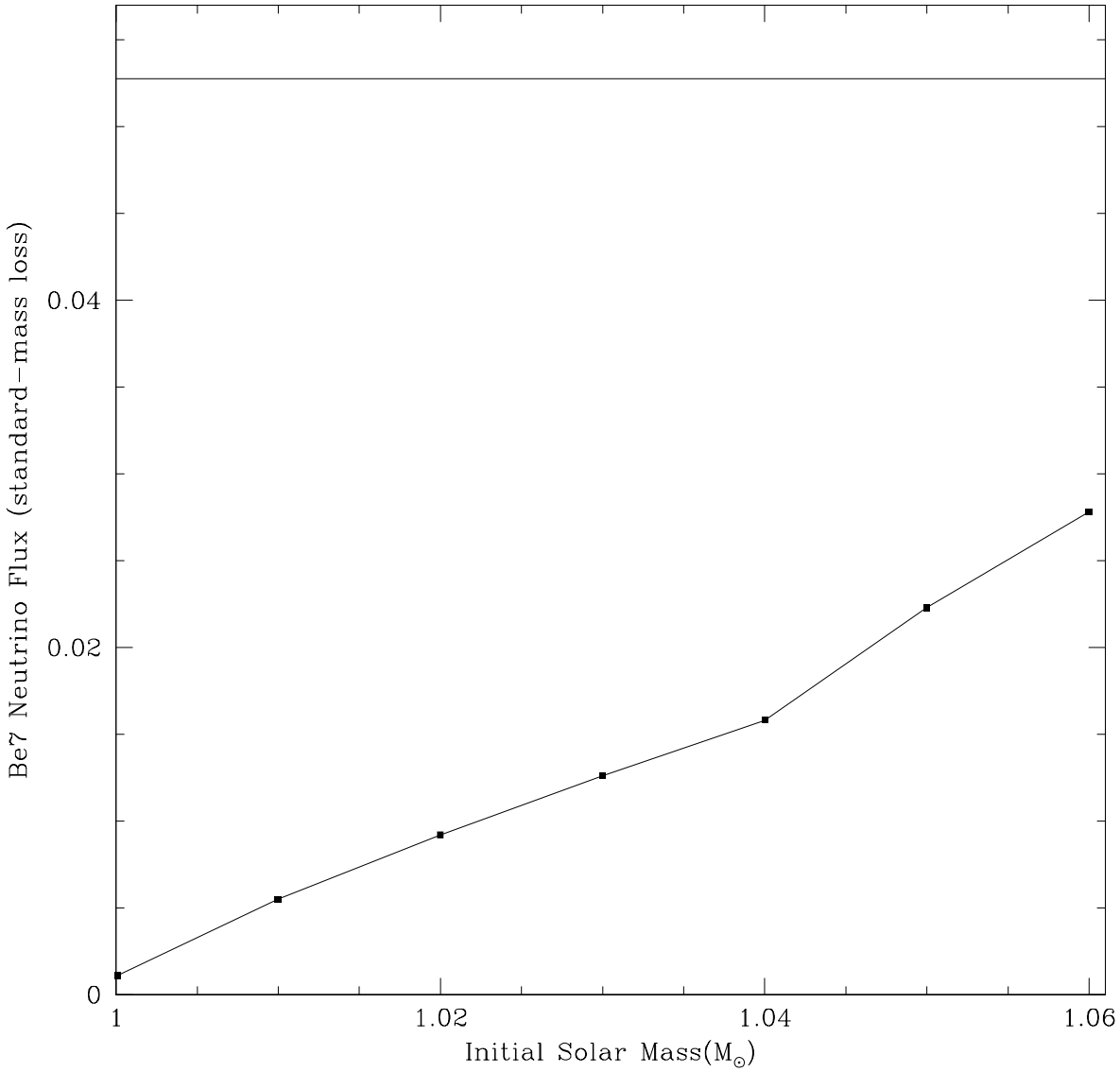

Fig. 12.— This graph shows deviation of the beryllium-7 neutrino flux from the standard model versus initial solar mass for the constant mass loss cases. The straight line represents the derived uncertainty in the beryllium-7 neutrino flux.

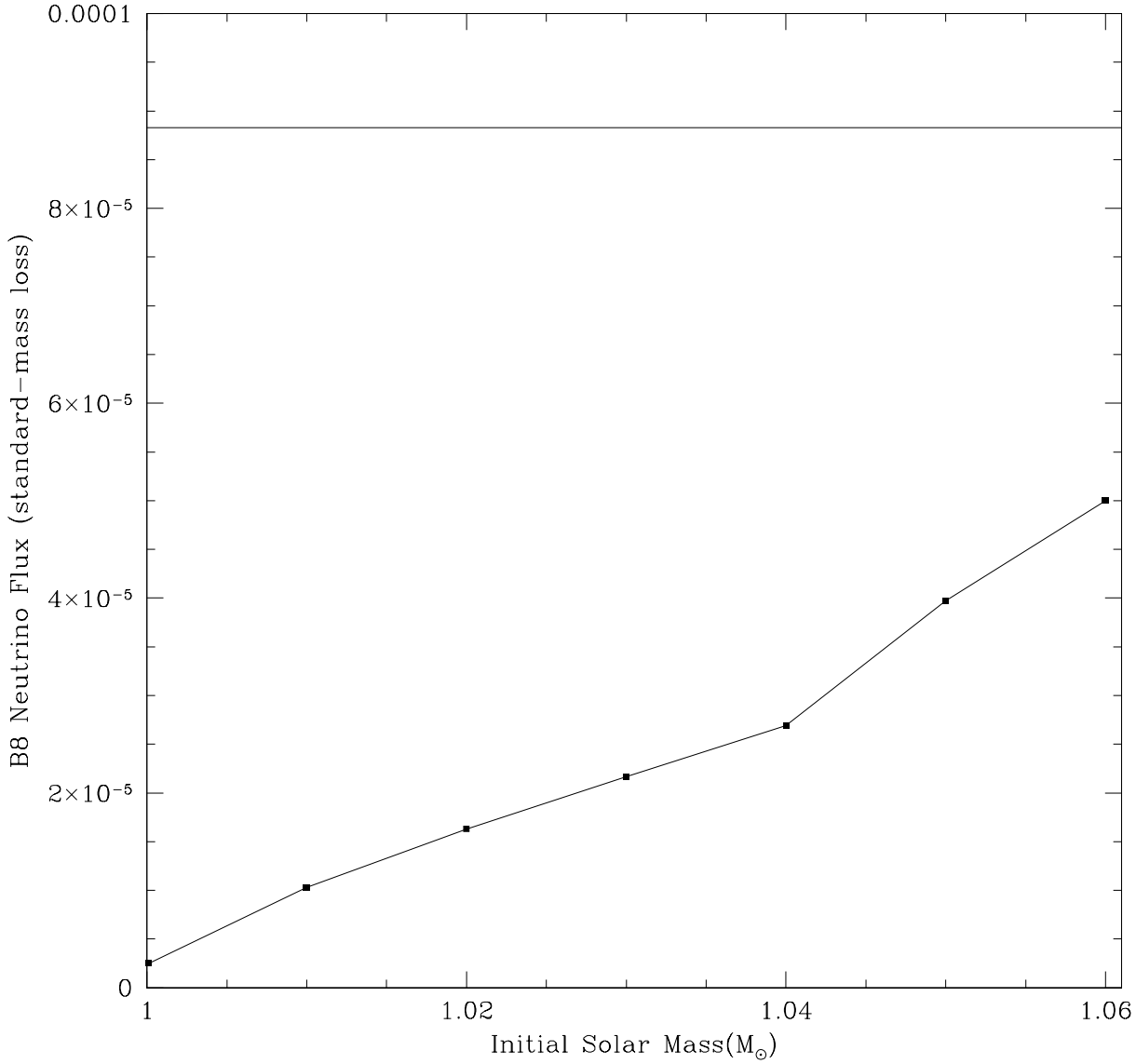

Fig. 13.— This graph shows deviation of the boron-8 neutrino flux from the standard model versus initial solar mass for the constant mass loss cases. The straight line represents the derived uncertainty in the boron-8 neutrino flux.

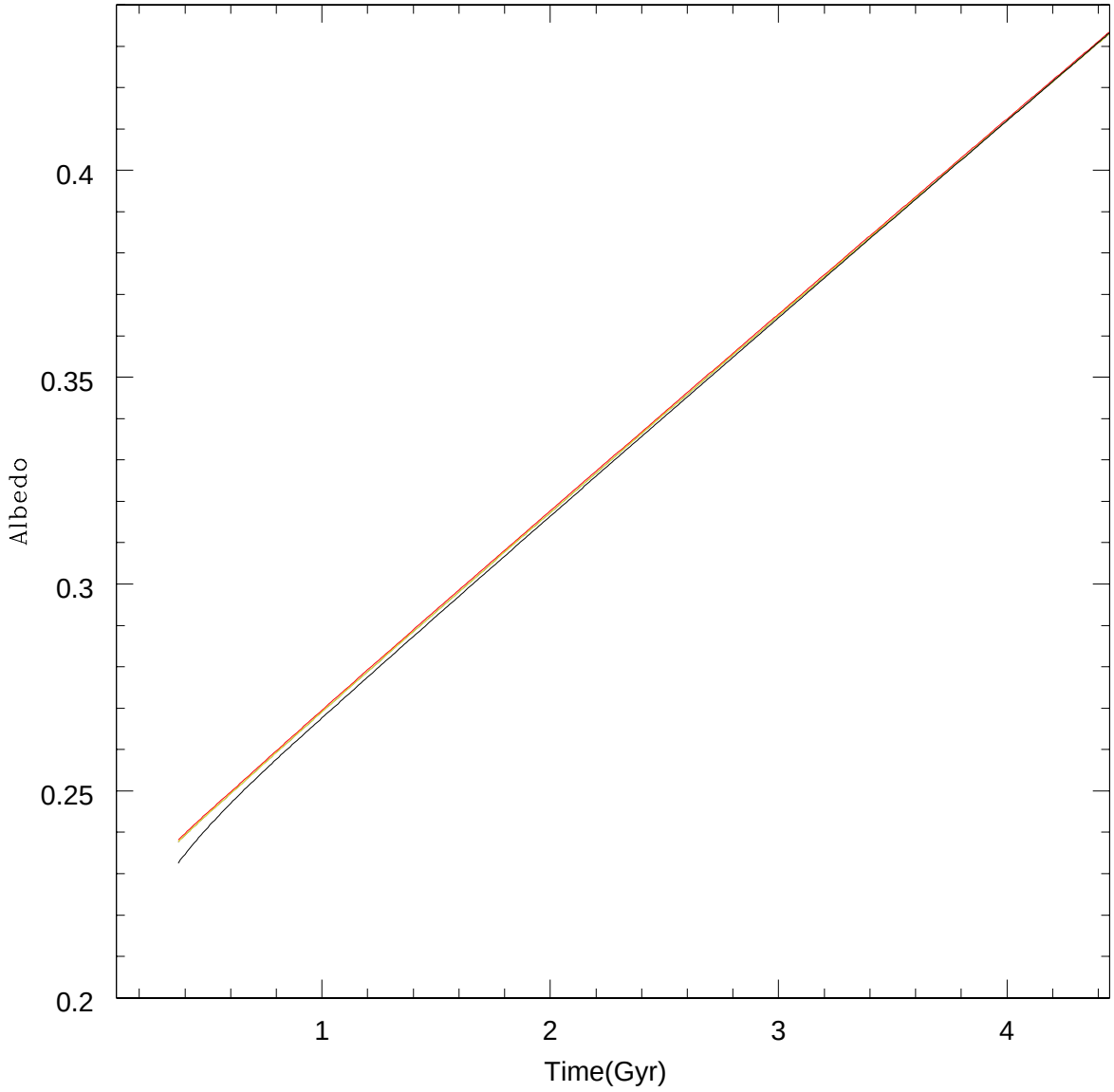

Fig. 14.— Albedo versus the infrared emissivity necessary to solve the faint young sun paradox for different physically motivated mass loss models. The lines are as follows: Black has no mass loss. Red has $P = 2$ according to Equation 2 and starts as a fast rotator Blue has $P = 3$ according to Equation 2 and starts as a fast rotator Yellow has $P = 3$ according to Equation 2 and starts as a slow rotator